Computing Flows Around Microorganisms: Slender-Body Theory and Beyond

Hoa Nguyen, Ricardo Cortez, and Lisa Fauci

Abstract. We present the mathematical framework that governs the interaction of a force-generating microorganism with a surrounding viscous fluid. We review slender-body theories that have been used to study flagellar motility, along with the method of regularized Stokeslets. We investigate the role of a dinoflagellate transverse flagellum as well as the flow structures near a choanoflagellate.

1. INTRODUCTION. Microorganisms move through fluid in an inertia-free world where their motile forces perfectly balance fluid forces at each instant [**38**]. If the flagellum of a sperm suddenly stops waving, the sperm cell does not continue coasting—the surrounding fluid motion and the sperm cell suddenly stop as well. Nevertheless, microorganisms have evolved to move about efficiently in this regime, using molecular motors that rotate, flex, or undulate one or more flagella. Figure 1(a,b,c,d) shows a sample of the diversity of flagellated eucaryotic microbes: the single flagellum of a rat spermatozoa [**33**], the transverse and longitudinal flagella of a dinoflagellate, the single flagellum of a choanoflagellate surrounded by a collar of microvilli [**10**], and the two anterior flagella of an algal cell [**46**]. These elastic, flexible appendages exert forces on the surrounding fluid, but at the same time, their shape responds to the fluid forces, a fully coupled mechanical system. The rat spermatozoa must make its way through the female reproductive tract and perhaps respond to chemical cues that guide its path [**13**]. The choanoflagellate, when it is attached to the substratum with a stalk, uses its flagellum to generate feeding currents [**10, 39**]. Figure 1(e) shows a diatom chain [**47**] that, like the dinoflagellate in Figure 1(b), is a type of phytoplankton. Phytoplankton are responsible for much of the oxygen production on Earth. Unlike the dinoflagellate, the diatom chain is nonmotile and is moved passively by the surrounding fluid [**47**]. In all cases, it is clear that the fluid dynamics near the microorganism is a vital contributor to its function.

The first mathematical formulation of the fluid dynamics of microorganism motility was given in the classic 1951 paper by G.I. Taylor [**43**]. Using asymptotic analysis, it was shown that a small-amplitude sinusoidal traveling wave passed down an infinite, periodic filament immersed in a two-dimensional viscous fluid would experience a translational velocity that was second order in amplitude. In the decades since, research on the hydrodynamics of microorganism motility has flourished. Along with laboratory experiments, mathematical modeling combined with analysis and computational methods has shed light on many features of coupled fluid-microorganism systems (see, for example, the review articles [**14, 17, 20, 29**]). Moreover, because of the revolution in microfluidic technologies [**42**], researchers are able to investigate the intriguing possibility of using microscale machines to move colloids or particles within a microfluidic device or *in vivo*. These microscale machines could be nature's own microorganisms [**46**], as in the algal cell of Figure 1(e) or a fabricated helical bacterium

http://dx.doi.org/10.4169/amer.math.monthly.121.09.810
MSC: Primary 92C10, Secondary 92C35; 92C17

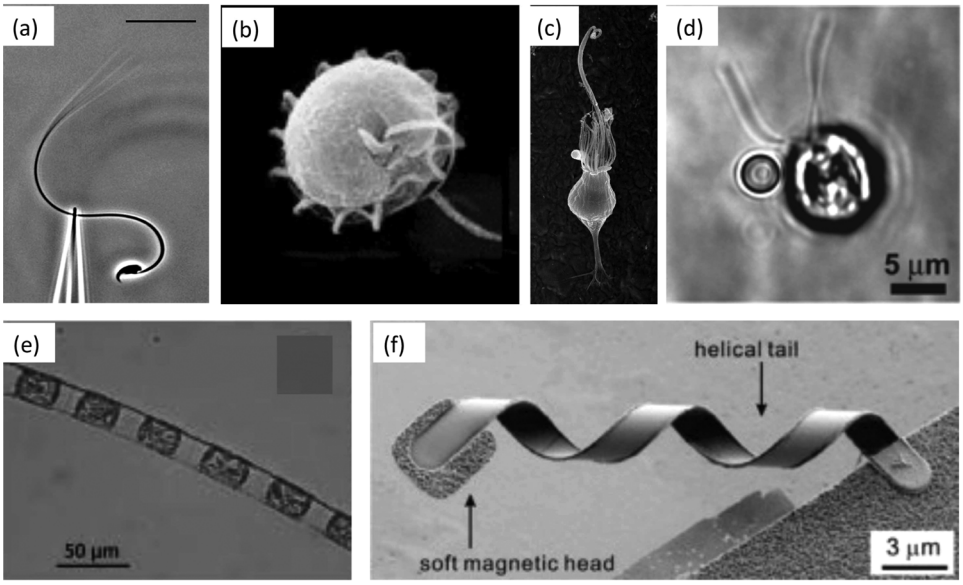

Figure 1. (a) A rat sperm flagellum being manipulated by a microprobe [**33**] (reprinted with permission from Charles Lindemann, taken from his website, `http://www2.oakland.edu/biology/lindemann/Clips.htm`). The scale bar is 20 microns. (b) The dinoflagellate *Pfisteria piscicida* (courtesy of the Aquatic Botany Lab, NC State). (c) Scanning electron micrograph of a choanoflagellate *Salpingoeca rosetta* thecate cell [**10**] (reprinted from *Developmental Biology*, **357** Cell differentiation and morphogenesis in the colony-forming choanoflagellate *Salpingoeca rosetta*, 72–82 (2011) with permission from Elevier). (d) A *Chlamydomonas reinhardtii* cell moving a polystyrene bead [**46**] (Copyright (2005) National Academy of Sciences, U.S.A.). (e) The chain-forming species of diatom *Lithodesmium undulatum* (courtesy of L. Karp-Boss, P. Jumars, and A. Young, University of Maine) [**47**] (Copyright 2014 by the Association for the Sciences of Limnology and Oceanography, Inc.). (f) A fabricated helical micromachine that will be actuated by an imposed electric field. Reprinted with permission from [**48**] (Copyright 2009 American Chemical Society).

that is driven by an applied magnetic field (Figure 1(f)) [**45, 48**]. As this technology to direct and control parcel delivery by microscale machines is developed, the importance of understanding flows around both natural and fabricated microorganisms is evident.

Here, we will present the mathematical framework that governs the interaction of a force-generating microorganism with the surrounding fluid. This framework gives rise to a linear relationship between the forces supported by the microorganism (no matter how complicated its geometry) and the fluid velocity, both at the microorganism's surface and around it. We will review slender body simplifications that exploit the aspect ratio of a typical flagellum, whose thickness is much smaller than its length. We will also describe the method of regularized Stokeslets that may be used for more complicated geometries that are not well approximated by a slender-body assumption. Using both slender-body theory and regularized Stokeslets, we will examine the rotational and translational motion of a waving helical ring chosen as a simple model for the transverse flagellum of a dinoflagellate. A higher fidelity model of a dinoflagellate, which includes the cell body, will also be discussed. Finally, we will present some computational simulations of the flow around choanoflagellates.

2. EQUATIONS OF MOTION. The governing equations of incompressible fluid dynamics express conservation of momentum and conservation of mass. Because the characteristic lengths and velocities for flows at the scale of microorganisms are so small, the fluid equations in this low Reynolds number regime reduce to the incompressible Stokes equations. In $\mathbb{R}^3$, they are

$$\mu \Delta \mathbf{u} = \nabla p - \mathbf{F}(\mathbf{x}, t) \tag{1}$$

$$\nabla \cdot \mathbf{u} = 0, \tag{2}$$

where μ is the dynamic fluid viscosity, $\mathbf{u}$ is the fluid velocity, p is the pressure, and $\mathbf{F}$ is the force that the microorganism is exerting on the fluid. This force will be concentrated at points corresponding to material points of the microorganism.

The first equation asserts that there is a balance between viscous forces, pressure forces and the forces exerted by the microorganism at each instant in time. This time-dependent force imposes a time scale in the flow. The second equation asserts that the fluid is incompressible. At every spatial position $\mathbf{x}$, for a given force $\mathbf{F}$, these are four scalar equations in four unknowns (the pressure and the three components of velocity). The pressure is determined by the incompressibility condition—by taking the divergence of (1), we see that the pressure satisfies the Poisson equation $\Delta p = \nabla \cdot \mathbf{F}$ in all of $\mathbb{R}^3$.

Most importantly, (1) and (2) represent a linear relationship between the forces exerted by the microorganism and the fluid velocity. In the study of the hydrodynamics of microorganism motility, one may exploit this linear relationship in either of two ways. If the kinematics of the organism due to a prescribed sequence of motions of the flagellum is assumed, then the velocities of the material points at the organism's surface, up to a rigid translation and rotation, are known. Given these prescribed velocities, the distribution of forces $\mathbf{F}$ along the surface that is required to produce these velocities may be solved. However, for a free-swimming organism, these forces must be such that the total force and torque generated must be zero. These six constraints are used to solve for the translational and rotational velocity of the microorganism (another six scalars). Alternatively, one may take as given the forces $\mathbf{F}$ exerted at the organism's surface. From such a distribution of forces, the resulting velocity field $\mathbf{u}$ may be calculated. Since the velocity of a material point of the microorganism is equal to the fluid velocity evaluated at that point, the translation and rotation of the microorganism is achieved by moving its surface points at these calculated velocities. In this second approach, the kinematics of motility are not prescribed but emerge from the fully coupled fluid-microorganism system. In this work, we will give two examples of the first approach, where the fluid flow and resulting swimming progression are calculated based upon the prescribed kinematics of both a dinoflagellate and a choanoflagellate flagellum.

3. SINGULARITY SOLUTIONS OF STOKES EQUATIONS. The fundamental solution of the problem in (1)–(2) is computed by considering an external force of the form $\mathbf{F}(\mathbf{x}) = \mathbf{f}\,\delta(\mathbf{x} - \mathbf{X})$, where δ is the Dirac delta distribution and $\mathbf{f}$ is a vector coefficient. We may solve for the pressure $p(\mathbf{x})$ and substitute it back into (1) to solve for the fluid velocity. The result is the Stokeslet [**36, 37**]:

$$p_S(\mathbf{x}) = \frac{\mathbf{f} \cdot (\mathbf{x} - \mathbf{X})}{4\pi |\mathbf{x} - \mathbf{X}|^3}, \tag{3}$$

$$\mathbf{u}_S(\mathbf{x}) = \frac{\mathbf{f}}{8\pi\mu|\mathbf{x} - \mathbf{X}|} + \frac{(\mathbf{f} \cdot (\mathbf{x} - \mathbf{X}))(\mathbf{x} - \mathbf{X})}{8\pi\mu|\mathbf{x} - \mathbf{X}|^3}. \tag{4}$$

We see that the velocity field due to this point force concentrated at $\mathbf{X}$ is, indeed, singular at $\mathbf{X}$, with a singularity $1/r$, where r is the distance from the point of evaluation of the Stokeslet to the position of the applied force. For such forces distributed on the surface of the microorganism, the Stokeslet kernel is integrable. However, we note that the Stokeslet kernel is not integrable over a one-dimensional curve in $\mathbb{R}^3$.

Other singularity solutions of the Stokes equations are derived from the Stokeslets by differentiation. For example, a dipole can be defined as the negative Laplacian of a Stokeslet of strength **D**:

$$\begin{aligned} p_D(\mathbf{x}) &= 0, \\ \mathbf{u}_D(\mathbf{x}) &= -\frac{2\mathbf{D}}{8\pi\mu|\mathbf{x}-\mathbf{X}|^3} + \frac{6(\mathbf{D}\cdot(\mathbf{x}-\mathbf{X}))(\mathbf{x}-\mathbf{X})}{8\pi\mu|\mathbf{x}-\mathbf{X}|^5}. \end{aligned} \tag{5}$$

Like the Stokeslet singular solution, the dipole singular solution satisfies the incompressibility condition ((2)) as well as $\mu\Delta\mathbf{u} = \nabla p$ at every spatial point $\mathbf{x} \neq \mathbf{X}$.

4. SLENDER-BODY THEORY. A slender-body theory begins with a thin tube immersed in Stokes flow and a distribution of singularity solutions along its centerline [**1, 9, 25, 27, 30, 31**]. Slender-body theories have been used to model the motion of cilia, flagella, and filaments in a variety of situations [**4, 19, 21, 22, 23, 26, 41, 43, 44**]. The boundary conditions associated with the flow are (a) $\mathbf{u}(\mathbf{x}) = \mathbf{v}(\sigma)$ for $\mathbf{x}$ on the surface of the slender body at the cross section labeled by the parameter σ, and (b) $\mathbf{u}(\mathbf{x}) \to 0$ as $|\mathbf{x}| \to \infty$. Here, $\mathbf{v}(\sigma)$ is a translational velocity of the cross section at σ. The centerline of the tubular body is assumed to have length L and parametrized by $\mathbf{X}(\sigma)$. Here, for simplicity, we consider a tube with constant radius a (see Figure 2). This tube is considered a slender body if the parameter $\epsilon = a/L$ is small. In dimensionless variables, the slender body has length 1 and tube radius $\epsilon \ll 1$. The goal of slender-body theory is to develop an asymptotic formula that relates the velocity of the slender body's surface to forces, exerted along its centerline, that is consistent with that motion. To this end, one considers the superposition of Stokeslets and dipoles, given in (4)-(5), distributed along the centerline

$$8\pi\mu\mathbf{u}(\mathbf{x}) = \int_0^1 \frac{\mathbf{f}(\sigma)}{r} + \frac{(\mathbf{f}(\sigma)\cdot\mathbf{r})\mathbf{r}}{r^3} - \frac{2\mathbf{D}(\sigma)}{r^3} + \frac{6(\mathbf{D}(\sigma)\cdot\mathbf{r})\mathbf{r}}{r^5} d\sigma, \tag{6}$$

where $\mathbf{r} = \mathbf{x} - X(\sigma)$ and $r = |\mathbf{r}|$. The strength of the dipoles will be chosen so that the velocities on a given circular cross section are approximately constant.

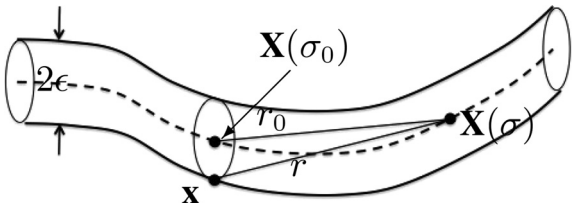

Figure 2. Schematic of a portion of the slender body. All spatial variables are scaled by the tube length so that ϵ is a dimensionless slenderness parameter.

The zeroth order approximation. We consider first a straight cylinder aligned with the x-axis so that $\mathbf{X}(\sigma) = (\sigma, 0, 0)$ and assume the forces and dipole strengths are constant along the section of the tube $\sigma \in [-q, q]$ with $\epsilon \ll q$. The velocity due to this section of the tube at surface point $\mathbf{x} = (\sigma_0, \epsilon\cos\theta, \epsilon\sin\theta)$ with $|\sigma_0| < q$ is

$$\begin{aligned} 8\pi\mu v_i(\sigma_0) = f_j \int_{-q}^{q} \frac{\delta_{ij}}{((\sigma_0-\sigma)^2+\epsilon^2)^{1/2}} + \frac{r_i r_j}{((\sigma_0-\sigma)^2+\epsilon^2)^{3/2}} d\sigma \\ + D_j \int_{-q}^{q} \frac{-2\delta_{ij}}{((\sigma_0-\sigma)^2+\epsilon^2)^{3/2}} + \frac{6 r_i r_j}{((\sigma_0-\sigma)^2+\epsilon^2)^{5/2}} d\sigma, \end{aligned}$$

with $r_i = \mathbf{x}_i - \mathbf{X}_i(\sigma)$ and implied summation notation. The second term of each integral involves the factor $r_i r_j$, which leads to a θ dependence of the velocity of the tube. That is, the velocity is different at different surface points on the same cross section of the tube. The θ dependence can be eliminated from the leading order terms of the integrals by choosing $\mathbf{D} = -\epsilon^2\mathbf{f}/4$. With this choice, taking $\beta = 4(q^2 - \sigma_0^2)/\epsilon^2$, the velocity above is (to leading order in ϵ/q)

$$8\pi\mu\mathbf{v}(\sigma_0) = \begin{pmatrix} 2\log\beta - 2 & 0 & 0 \\ 0 & \log\beta + 1 & 0 \\ 0 & 0 & \log\beta + 1 \end{pmatrix} \begin{pmatrix} f_1 \\ f_2 \\ f_3 \end{pmatrix}. \tag{7}$$

In *resistive force theory*, a long tube is approximated by a series of straight cylindrical pieces placed end to end, and the velocity of each cylindrical piece is computed from (7). This local slender-body theory was used in the classic 1955 work by Gray and Hancock to study sperm motility [**19**]. Additional details can be found in [**3, 31**].

We note that as the evaluation point on the surface approaches an endpoint of the tube (i.e., as $\sigma_0 \to \pm q$), the approximation above becomes singular. This is a manifestation of the fact that the approximation degrades as the evaluation point approaches the tube endpoints. Higher-order singularities can be included to improve the expressions [**25**]. In the case of a periodic slender body, the centerline parametrization can be chosen so that the evaluation point is always at $\sigma_0 = 0$, leading to a simpler expression.

Lighthill's theory. We consider first a construction of the slender-body velocity following the strategy in [**24, 30, 31**]. The velocity evaluated at a point $\mathbf{x}$ is given by (6) with $\mathbf{D}(\sigma) = -\epsilon^2\mathbf{f}(\sigma)/4$. The result is

$$8\pi\mu\mathbf{u}(\mathbf{x}) = \int_0^1 \frac{\mathbf{f}(\sigma)}{r} + \frac{(\mathbf{f}(\sigma)\cdot\mathbf{r})\mathbf{r}}{r^3} + \frac{\epsilon^2\mathbf{f}(\sigma)}{2r^3} - \frac{3\epsilon^2(\mathbf{f}(\sigma)\cdot\mathbf{r})\mathbf{r}}{2r^5} d\sigma,$$

where $\mathbf{r} = \mathbf{x} - \mathbf{X}(\sigma)$ and $r = |\mathbf{r}|$. The choice of $\mathbf{D}(\sigma)$ is motivated by the arguments in the zeroth order approximation theory that eliminate the dependence on the angle θ from the leading order terms of the integrals. The goal is to let $\mathbf{x}$ approach a point on the tube centerline $\mathbf{X}(\sigma_0)$. To do this, the integral is divided into two pieces. The near-field portion is where $|\sigma - \sigma_0|$ is small, the forces are constant and equal to $\mathbf{f}(\sigma_0)$, and the tube is assumed to be straight. In the far-field portion, the dipole is neglected due to its faster decay in r. Combining these elements, we obtain a final expression

$$8\pi\mu\mathbf{v}(\sigma_0) = 2\mathbf{f}_n(\sigma_0) + \int_{\rho<r_0} \frac{\mathbf{f}(\sigma)}{r_0} + \frac{(\mathbf{f}\cdot\mathbf{r}_0)\mathbf{r}_0}{r_0^3}\, d\sigma, \tag{8}$$

where $\mathbf{r}_0 = \mathbf{X}(\sigma_0) - \mathbf{X}(\sigma)$, $r_0 = |\mathbf{r}_0|$ and $\rho = \epsilon\sqrt{e}/2$. The factor $\mathbf{f}_n$ is the component of $\mathbf{f}$ normal to the tube centerline. In Lighthill's slender-body theory, the errors are $O(\epsilon)$.

Keller–Rubinow theory. Keller and Rubinow's theory [**28**] develops the relationship between velocity and force with errors $O(\epsilon^2\ln(\epsilon))$. They begin by approximating (6) at a point $\mathbf{x}$ in the fluid far from the filament. The far-field expression neglects the dipoles as they decay faster than the Stokeslets. Then, as before, (6) is approximated at a point $\mathbf{x}_0$ in the fluid near the point $\mathbf{X}(\sigma_0)$ on filament using $\mathbf{D} = -\epsilon^2\mathbf{f}/4$. In the near

field, the tube is assumed to have a uniform force density and a negligible curvature, leading to the local term

$$8\pi\mu\mathbf{u}(\mathbf{x}_0) = 8\pi\mu\mathbf{v}(\sigma_0) - (\mathbf{f}_n + 2\mathbf{f}_\tau)\left[\ln\left(\frac{|\mathbf{x}_0|^2}{\epsilon^2}\right) + \frac{|\mathbf{x}_0|^2 - \epsilon^2}{|\mathbf{x}_0|^2}\right] + 2\mathbf{f}_\tau\left[\frac{|\mathbf{x}_0|^2 - \epsilon^2}{|\mathbf{x}_0|^2}\right] + 2(\mathbf{f}_0 \cdot \mathbf{x}_0)\mathbf{x}_0\left[\frac{|\mathbf{x}_0|^2 - \epsilon^2}{|\mathbf{x}_0|^4}\right],$$

where $\mathbf{f}_0 = \mathbf{f}(\sigma_0)$, $\mathbf{f}_n$ and $\mathbf{f}_\tau$ are the components of $\mathbf{f}(\sigma_0)$ normal and tangential to the tube centerline, and $\mathbf{v}(\sigma_0)$ is the unknown filament velocity at $\mathbf{X}(\sigma_0)$. This expression is matched asymptotically with the far-field velocity to produce a formula for the filament velocity at $\mathbf{X}(\sigma_0)$

$$8\pi\mu\mathbf{v}(\sigma_0) = \int_0^1 \frac{\mathbf{f}(\sigma)}{r_0} + \frac{(\mathbf{f}(\sigma)\cdot\mathbf{r}_0)\mathbf{r}_0}{r_0^3} - \frac{\mathbf{f}(\sigma_0) + (\mathbf{f}(\sigma_0)\cdot\mathbf{s})\mathbf{s}}{|\sigma - \sigma_0|}\, d\sigma + (\mathbf{f}_n + 2\mathbf{f}_\tau)\left[\ln\left(4\sigma_0(1-\sigma_0)/\epsilon^2\right) - 1\right] + 2\mathbf{f}_n(\sigma_0), \tag{9}$$

where $\mathbf{r}_0 = \mathbf{X}(\sigma_0) - \mathbf{X}(\sigma)$, $r_0 = |\mathbf{r}_0|$, and $\mathbf{s}$ is a unit vector tangent to the filament at $\mathbf{X}(\sigma_0)$. Because the asymptotic matching has been done for a point in the fluid, the Keller–Rubinow theory also provides an expression for the fluid motion. More details can also be found in [**44**].

5. REGULARIZED STOKESLETS. The Keller–Rubinow slender-body formulation [**28**] relies on the exact cancellation of integrals that have the same asymptotic singularity, which is difficult to achieve computationally unless one regularizes the integration kernel [**44**]. More generally, the Stokeslet formula gives a singular velocity field when the forces are distributed along curves or scattered points. This motivates revisiting the Stokes equations in (1)–(2) with a modified model of the forces.

We consider a force that is distributed smoothly over a small sphere of radius δ. Rather than a delta distribution, the force is given by $\mathbf{F}(\mathbf{x}) = \mathbf{f}\phi_\delta(|\mathbf{x} - \mathbf{X}|)$, where $\phi_\delta(r)$ is a smooth symmetric function with total integral equal to 1 (like a narrow Gaussian). The regularization parameter δ controls the width of the function. The function $\phi_\delta(r)$ can be selected so that $\Delta G_\delta = \phi_\delta$ and $\Delta B_\delta = G_\delta$ can be solved analytically for $G_\delta(r)$ and $B_\delta(r)$. Using these definitions, the solution of

$$\mu\Delta\mathbf{u} = \nabla p - \mathbf{f}\phi_\delta(|\mathbf{x} - \mathbf{X}|)$$
$$\nabla\cdot\mathbf{u} = 0,$$

for the specific regularizing function $\phi_\delta(r) = 15\delta^4/8\pi(r^2+\delta^2)^{7/2}$ is

$$p_S^\delta(\mathbf{x}) = \mathbf{f}\cdot(\mathbf{x} - \mathbf{X})\,\frac{(2r^2 + 5\delta^2)}{8\pi\mu(r^2+\delta^2)^{5/2}}, \tag{10}$$

$$\mathbf{u}_S^\delta(\mathbf{x}) = \frac{\mathbf{f}\,(r^2 + 2\delta^2)}{8\pi\mu(r^2+\delta^2)^{3/2}} + \frac{(\mathbf{f}\cdot(\mathbf{x}-\mathbf{X}))(\mathbf{x}-\mathbf{X})}{8\pi\mu(r^2+\delta^2)^{3/2}}, \tag{11}$$

where $r = |\mathbf{x} - \mathbf{X}|$. As before, other regularized solutions to Stokes equations can be found by differentiation. The method of regularized Stokeslets has been used in many

applications related to the simulation swimming motions of microorganisms [**5, 7, 16, 18, 40**].

The regularized Stokeslet pressure and velocity in (10)–(11) are exact solution to Stokes equations due to the regularized force centered at $\mathbf{X}$ and are no longer singular; the velocity is exactly incompressible, and the expressions reduce to the singular Stokeslet in (3)–(4) as $\delta \to 0$. Using this method of regularized Stokeslets [**6, 7**], one may readily compute the velocities at a collection of points on a surface due to forces exerted at those same points by summing up the resulting regularized Stokeslets because the Stokes equations are linear. Alternatively, one may invert this relationship to compute the forces at the points that give rise to prescribed velocities at these points. Once these forces are computed, the evaluation of the fluid velocity at any point in $\mathbb{R}^3$ is easily achieved by summing up the Stokeslets due to each of these forces in (11) evaluated at that spatial point. We remark that a slender-body assumption is not required.

If a slender-body assumption is valid, then one may still exploit the geometry by distributing regularized singularities along a centerline rather than around the surface of the tube. The slender-body theories of Lighthill and Keller–Rubinow were rederived in [**8**] for the case of force and dipole fields where the delta distribution was replaced by a smooth localized spherically symmetric function $\phi_\delta(r)$ centered at every point $\mathbf{X}(\sigma)$ of the body centerline, as above. Note that δ is assumed to satisfy $\delta \sim \epsilon$.

For example, the regularized Keller–Rubinow formula to the asymptotic order $O(\epsilon^2 \ln(\epsilon)) + O(\delta^2 \ln(\delta))$ becomes

$$8\pi\mu\mathbf{v}(\sigma_0) = \int_0^1 \frac{\mathbf{f}(\sigma)}{\sqrt{r_0^2+\delta^2}} + \frac{(\mathbf{f}(\sigma)\cdot\mathbf{r}_0)\mathbf{r}_0}{r_0^2\sqrt{r_0^2+\delta^2}} - \frac{\mathbf{f}(\sigma_0)+(\mathbf{f}(\sigma_0)\cdot\mathbf{s})\mathbf{s}}{\sqrt{t^2+\delta^2}}\, d\sigma$$

$$+ (\mathbf{f}_0 + (\mathbf{f}_0\cdot\mathbf{s})\mathbf{s})\big[\ln(4\sigma_0(1-\sigma_0)/(\epsilon^2+\delta^2)) - 1\big] + 2\mathbf{f}_n(\sigma_0), \quad (12)$$

where $\mathbf{r}_0 = \mathbf{X}(\sigma_0) - \mathbf{X}(t)$. While the standard theory is recovered as $\delta \to 0$, the final expression has built-in smoothing that eliminates instabilities encountered in computations with unsmoothed formulas (see [**8**] for details).

Regardless of the slender-body theory used in computations, the integrals in (8), (9), or (12) are approximated by discretizing the centerline of the slender body and replacing the integral with a quadrature rule. In practice, when the kinematics are imposed, the forces at the discrete points on the centerline are computed by solving a linear system of equations since the velocities at these same points are known.

6. EXAMPLES.

Function of the dinoflagellate transverse flagellum. Dinoflagellates are unicellular phytoplankton that swim due to the action of two flagella (see Figure 1(b)). A trailing, longitudinal flagellum that propagates approximately planar waves, much like a sperm flagellum, and a transverse helical flagellum that is wrapped around the cell's equator and propagates helical waves. The swimming trajectories of dinoflagellates are helical, and the cell is observed to rotate about its longitudinal axis and translate also along this axis. Until recently, there were differing conclusions about the role of the each of the flagella [**15, 32**]. For instance, is the helical transverse flagellum responsible for rotation about the cell's axis or translation along the axis or both? In order to address this question, in [**34**], we idealized the transverse flagellum by a closed cylindrical ring around which helical bending waves were propagated. Here, we revisit this idealized problem to compare Lighthill's slender-body calculations of rotational and translational velocity to those calculated using the method of regularized Stokeslets.

We prescribe the kinematics of the tubular helical ring, such that its centerline's position at time t is

$$\begin{cases} X(s,t) = \left[r - R\sin\left(\frac{2\pi s}{\lambda} - \omega t\right)\right]\cos\left(\frac{s}{r}\right) \\ Y(s,t) = \left[r - R\sin\left(\frac{2\pi s}{\lambda} - \omega t\right)\right]\sin\left(\frac{s}{r}\right) \\ Z(s,t) = R\cos\left(\frac{2\pi s}{\lambda} - \omega t\right) \end{cases} \tag{13}$$

where $0 \le s \le 2\pi r = L$. The axis of this circular helix is a baseline circle of radius r in the plane $z = 0$. The helical amplitude is R and λ is the wavelength. The surface of the helical ring is then formed by circular cross sections of radius r_h placed normal to the above centerline. As time t progresses, a traveling wave with speed $w_s = \frac{\omega\lambda}{2\pi}$ revolves around the ring. In the following, we report lengths scaled by the diameter of the baseline circle $2r$, which we take equal to one, and velocities scaled by the velocity of the traveling wave.

Figure 3 shows two views of a slender ring whose baseline circle has diameter $2r = 1$, tubular radius is $r_h = 0.035$ with four pitches supported along the ring and a helical amplitude of $R = 0.09$, wavelength is $\lambda = \frac{2\pi r}{4}$, and angular frequency is $\omega = 0.1$. Using the method of regularized Stokeslets, the forces that are consistent with the prescribed kinematics, along with the translational and rotational velocity that guarantee that momentum and angular momentum are conserved, were computed. The surface of the waving ring was discretized using 120 cross sections with six nodes per cross section. The average distance between neighboring points on the ring's surface was $ds = 0.0325$, and the blob size was chosen to be $\delta = 0.019$. Figure 3 shows streamlines that are projected onto the given planes by computing the 3D fluid velocities on these planes due to the computed force distribution on the surface of the ring. Note the upward-welling flow at the ring's center. In these streamline plots, it is not possible to discern either the translational or rotational velocity of the ring that will perfectly balance force and torque. We report both the rotational velocity of the ring (V_r) about its axis and the upwards translational velocity normal to the ring's baseline circle (V_t) as a function of amplitude in Figure 4. We find that, indeed, a wave passed around the helical ring causes it to undergo both rotation about its axis and translation along its axis. Whether it moves upward or downward is dictated by the handedness of the helix and the direction of the traveling wave. Figure 4 shows that both rotational and translational velocities increase with the amplitude of the helical wave. In this log-log plot, a line of slope two is included to demonstrate that these velocities are second order in amplitude for small amplitudes. We also note an excellent agreement between the velocities computed using regularized Stokeslets and those computed using Lighthill's slender-body theory. In fact, the translational velocities computed using both methods are basically identical. We remark that while the method of regularized Stokeslets relies on computing forces at a discrete collection of points on the two-dimensional cylindrical surface, the slender-body method computes forces only at a discrete collection of points that discretize the one-dimensional helical centerline.

Of course, this idealized helical ring, while shedding some light on the function of the transverse flagellum of a dinoflagellate, tells only a part of the story. What happens when this ring is wrapped around a cell body? Will it still rotate as well as translate along its axis? In order to examine this, we added a spherical cell body, centered also at the ring's center. Figure 5(a) shows a sphere whose radius $\bar{R} = .5(r - R - 1.5r_h)$ and the sphere with twice that radius in Figure 5(b). Because this structure no longer satisfies the assumptions of slender-body theory, we use the method of regularized Stokeslets to compute the rotational and translational velocities of the coupled cell-flagellum system. The surface of the sphere is discretized using a spherical centroidal

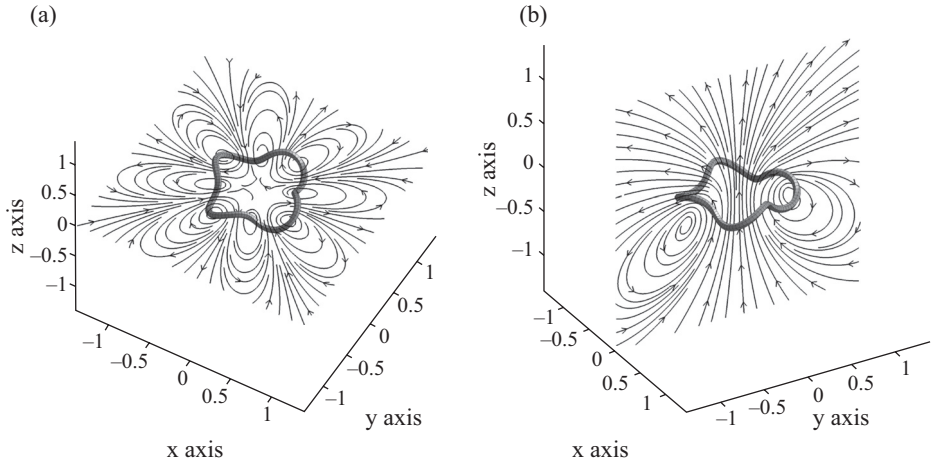

Figure 3. Flow around the helical ring on (a) the xy-plane and (b) the yz-plane. These streamlines are projections onto the given planes of the 3D velocities calculated on those planes using the method of regularized Stokeslets.

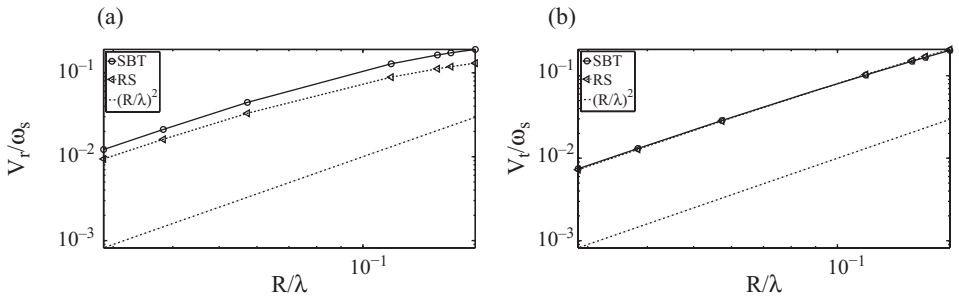

Figure 4. Log-log plots of (a) normalized rotational velocity (V_r/ω_s) versus (R/λ) and (b) normalized translational velocity (V_t/ω_s) versus (R/λ) computed using slender-body theory (SBT) and regularized Stokeslets with prescribed wave kinematics (RS).

Voronoi tessellation [**12**] so that points are approximately equally spaced with the average distance between nearby points about ds on the ring's surface. Points on the surface of the waving ring will move with a superposition of two velocities—the velocity of the ring relative to itself due to the prescribed kinematics in Equation (13) and the velocity due to a rigid translation and rotation. The points on the surface of the sphere do not move relative to each other. Therefore, we specify the velocities due to shape changes on the waving ring as before but prescribe zero shape-change velocity at all points on the sphere. We then balance the total forces and torques on the combined cell-flagellum structure to calculate the translational and rotational velocity of the structure. Figure 6(a) shows that the resulting normalized rotational velocity decreases with increasing spherical radius. However, Figure 6(b) shows that the translational velocity along its axis actually increases with spherical radius. In fact, the translational velocity of the structure in Figure 5(b) is about 33% larger than that of the helical ring alone. The rotational velocity, on the other hand, is about 19% smaller. Note that the sphere in Figure 5(a) is discretized with 450 points (the average distance between nearby points is 0.0329) while the sphere in Figure 5(b) is discretized with 1800 points (the average distance between nearby points is 0.0332). We also choose a blob size $\delta = 0.019$ as in the case without the sphere.

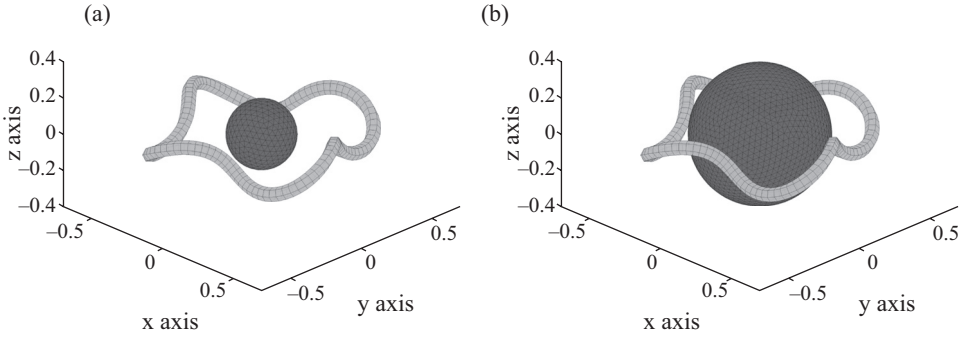

Figure 5. 3D view: Four-pitch helical ring of baseline-circular radius r, helical amplitude R and cross-sectional radius r_h, enclosing a sphere of radius $0.5\bar{R}$ in (a) and of radius $\bar{R}$ in (b) where $\bar{R} = r - R - 1.5r_h$. The sphere is discretized using spherical centroidal Voronoi tessellations in Du et al. [**12**].

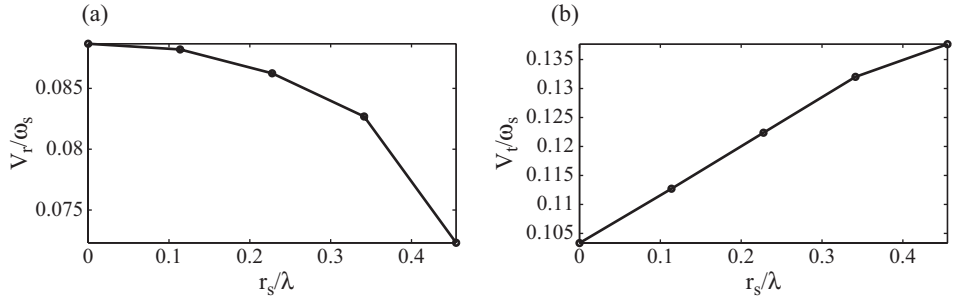

Figure 6. Plots of (a) normalized rotational velocity (V_r/ω_s) versus normalized spherical radius (r_s/λ) and (b) normalized translational velocity (V_t/ω_s) versus normalized spherical radius (r_s/λ) computed using regularized Stokeslets with prescribed wave kinematics.

Flows around choanoflagellates. Choanoflagellates are microorganisms whose life cycle may include stages as a solitary, single cell as well as stages where it is part of a multicelled colony. It is believed that understanding the aspects of multicellularity in this model system can give insight into the evolution of cell differentiation in animals. The choanoflagellate *Salpingoeca rosetta*, in response to different environmental cues, differentiates into cell types that are either single celled or in colonies in the form of chains or rosettes [**10**]. Each of the single-celled microorganisms has a single flagellum that is responsible for motility and creating a fluid flow that draws bacterial prey onto the outer surface of its collar of microvilli (see Figure 1(c)). Free-swimming cells may have a full collar that is about 5 microns long, a truncated collar, or none at all. Chain colonies are formed with cells attached side-by-side, but rosette colonies are formed when the cells aggregate around a central point, with their flagella emanating radially outwards from the spherical colony. In the intriguing experiments of Dayel et al. [**10**], swimmer cells are induced into forming rosette colonies when bacteria are introduced to the culture. Why is colony formation advantageous? Does the cooperative arrangement of flagella of the cells, either side-by-side or emanating radially from a sphere, enhance fluid flow to the cells? Recently, Roper et al. [**39**] investigated the hydrodynamics of flagellated cells in a colony using a minimal fluid model, where each cell is represented by two point forces. Studying the flow generated by these singularities sufficiently far away from the cell dimers, it was shown that enhanced fluid supply does occur. In this minimal model, neither the details of the flow near the organism nor the effects of its morphologies are addressed.

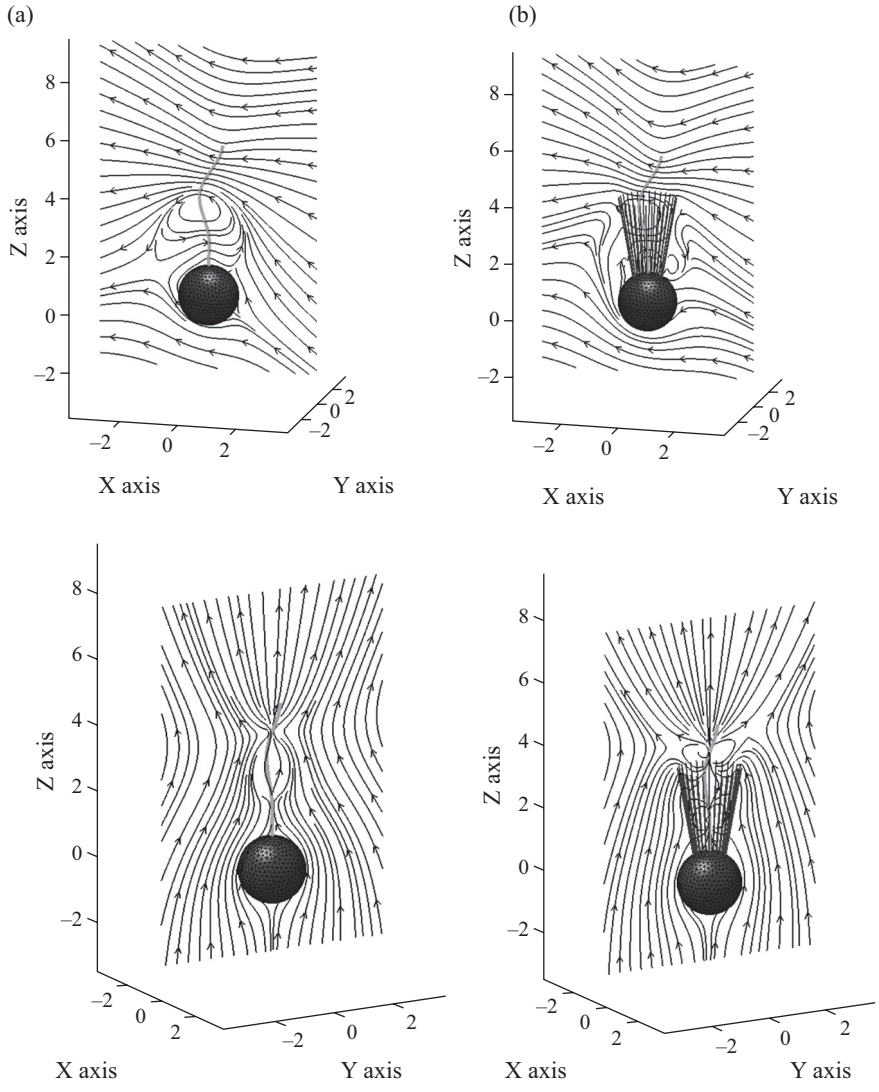

Figure 7. Projected streamlines around the choanoflagellate model on the xz-plane (first row) and the yz-plane (second row) for an organism without microvilli (column (a)) and with microvilli (column (b)). A sinusoidal wave from cell body to tip is being passed along the planar flagellum in the xz-plane.

In an effort to understand the role of the microvilli collar in the flow around a single choanoflagellate, either tethered in space or freely swimming, we use the method of regularized Stokeslets. The surface of a spherical cell body, individual microvilli, and the flagellum that is beating in a planar wave from cell body to tip are discretized. The velocity on the flagellum is imposed based upon the prescribed wave kinematics. Zero fluid velocity on the cell body and on the microvilli is also imposed. Because the cell body is fixed in space, as for a thecate cell, we do not allow for a translational and rotational velocity. Figure 7 shows four snapshots of projected streamlines for a cell without microvilli (column a) and a cell with microvilli (column b). The planar flagellum is undulating sinusoidally in the xz-plane. While the flow away from the microorganism is similar in each case, the flow nearby is certainly altered when microvilli are present. It is this nearby flow that dominates the dynamics of nutrient uptake at the

cell surface. It is our hope to expand this model to study the hydrodynamic interaction of a collection of such cells in a colony. In particular, we expect that detailed models like these can be used to inform the more minimal models as in [**39**].

7. DISCUSSION. Here, we have presented an overview of the mathematics central to computing flows around microorganisms. Because the flagella of these small creatures are much longer than they are thick, the applied mathematician's quest for a small parameter ends in triumph. Slender-body theories have been succesfully used to study flagellar hydrodynamics. However, the diversity of microorganisms, with their many flagella and other appendages, quickly moves beyond the realm of slender-body assumptions. Other formulations, like the method of regularized Stokeslets, have been developed to address these complications.

It is important to note that the dinoflagellate and choanoflagellate examples chosen above assumed that the kinematics of the waving flagella were preset and not determined by the coupling to the viscous fluid around them. In fact, many challenging questions in the hydrodynamics of microorganism motility evolve around understanding how passive elastic forces and forces due to molecular motors interact with the surrounding fluid to achieve the observed wave form. How and why do the flagella of a bacteria form a bundle [**2**]? Why does the symmetric beat pattern of a mammalian sperm change to a highly asymmetric one when it is about to fertilize the egg [**11**]? The methodology described above is also perfect for these questions (i.e., [**16, 35**])—here, the forces are specified and the resulting velocities are directly evaluated. However, this brings up a whole other set of mathematical modeling challenges. What are the elastic properties of the microorganisms and their flagella? What are the internal force generating mechanisms that enable flagellar beating, and how are they altered by biochemistry or mechanics?

In summary, the fluid dynamics of microorganism motility has been a driving force in applied mathematics and computation. With the advance of technologies, both experimental and computational, understanding movement at this microscale is possible. Of course, as more is learned, more questions are posed, presenting a rich array of intriguing problems for mathematical scientists.

ACKNOWLEDGMENT. The authors thank the undergraduate student Niti Nararidh for productive summer research work on the choanoflagellate project.

REFERENCES

1. G. K. Batchelor, Slender-body theory for particles of arbitrary cross-section in Stokes flow, *J. Fluid Mech.* **44** (1970) 419–440.
2. H. Berg, R. Anderson, Bacteria swim by rotating their flagellar filaments, *Nature* **245** (1973) 380–382.
3. J. R. Blake, E. O. Tuck, P. W. Wakeley, A note on the S-transform and slender body theory in Stokes flow, *IMA J. Appl. Math.* **75** (2010) 343–355, `http://dx.doi.org/10.1093/imamat/hxq005`.
4. A. T. Chwang, T. Y. Wu, A note on the helical movements of micro-organisms, *Proc. Roy. Soc. Lond. B* **178** (1971) 327–346.
5. L. Cisneros, J. Kessler, R. Ortiz, R. Cortez, M. Bees, Unexpected bipolar flagellar arrangements and long-range flows driven by bacteria near solid boundaries, *Phys. Rev. Lett.* **101** (2008) 168102, `http://dx.doi.org/10.1103/physrevlett.101.168102`.
6. R. Cortez, The method of regularized Stokeslets, *SIAM J. Sci. Comput.* **23** (2001) 1204, `http://dx.doi.org/10.1137/s106482750038146x`.
7. R. Cortez, L. Fauci, A. Medovikov, The method of regularized Stokeslets in three dimensions: Analysis, validation, and application to helical swimming, *Phys. Fluids* **17** (2005) 031504.
8. R. Cortez, M. Nicholas, Slender body theory with regularized forces, *Commput. Appl. Math Comp. Sci.* **7** (2012) 33–62, `http://dx.doi.org/10.2140/camcos.2012.7.33`.

9. R. G. Cox, The motion of long slender bodies in a viscous fluid Part 1. General theory, *J. Fluid Mech.* **44** (1970) 791–810.
10. M. Dayel, R. Alegado, S. Fairclough, T. Levin, S. Nichols, K. McDonald, N. King, Cell differentiation and morphogenesis in the colony-forming choanoflagellate *Salpingoeca rosetta*, *Devel. Biol.* **357** (2011) 73–82, http://dx.doi.org/10.1016/j.ydbio.2011.06.003.
11. R. P. DeMott, S. S. Suarez, Hyperactivated sperm progress in the mouse oviduct, *Biol. Reprod.* **46** (1992) 779–785.
12. Q. Du, M. Gunzburger, L. Ju, Constrained centroidal Voronoi tessellations for surfaces, *SIAM J. Sci. Comput.* **24** (2003) 1488–1506.
13. M. Eisenbach, L. Giojalas, Sperm guidance in mammals—An unpaved road to the egg, *Nat. Rev. Mol. Cell Biol.* **7** (2006) 276–285, http://dx.doi.org/10.1038/nrm1893.
14. L. Fauci, R. Dillon, Biofluidmechanics of reproduction, *Annu. Rev. Fluid. Mech.* **38** (2006) 371–394.
15. T. Fenchel, How dinoflagellates swim., *Protist* **152** (2001) 329–338, http://dx.doi.org/10.1146/annurev.fluid.37.061903.175725.
16. H. Flores, E. Lobaton, S. Mendez-Diez, S. Tlupova, R. Cortez, A study of bacterial flagellar bundling, *Bull. Math. Bio.* **67** (2005) 137–168, http://dx.doi.org/10.1016/j.bulm.2004.06.006.
17. E.A.Gaffney, H.Gadelha, D.J.Smith, J.R.Blake, J.C.Kirkman-Brown, Mammalian sperm motility: Observation and theory, *Ann. Rev. Fluid Mech.* **43** (2011) 501–528.
18. E. A. Gillies, R. M. Cannon, R. B. Green, A. A. Pacey, Hydrodynamic propulsion of human sperm, *J. Fluid Mech.* **625** (2009) 445–474.
19. J. Gray, G. J. Hancock, The propulsion of sea-urchin spermatozoa, *J. Exp. Biol.* **32** (1955) 802–814.
20. J. S. Guasto, R. Rusconi, R. Stocker, Fluid mechanics of planktonic microorganisms, *Ann. Rev. Fluid Mech.* **44** (2012) 373–400, http://dx.doi.org/10.1146/annurev-fluid-120710-101156.
21. S. Gueron, N. Liron, Simulations of three-dimensional ciliary beats and cilia interactions, *Biophys. J.* **65** (1993) 499–507.
22. J. J. L. Higdon, The generation of feeding currents by flagellar motions, *J. Fluid Mech.* **94** (1979) 305–330.
23. ———, A hydrodynamic analysis of flagellar propulsion, *J. Fluid Mech.* **90** (1979) 685–711.
24. J. Lighthill, Helical distributions of Stokeslets, *J. Eng. Math.* **30** (1996) 35–78.
25. R. E. Johnson, An improved slender-body theory for Stokes flow, *J. Fluid Mech.* **99** (1980) 411–431.
26. R. E. Johnson, C. J. Brokaw, A comparison between resistive-force theory and slender-body theory, *Biophys. J.* **25** (1979) 113–127.
27. R. E. Johnson, T. Y. Wu, The asymptotic solution formula for uniform flow past a slender torus, *J. Fluid Mech.* **95** (1979) 263–277.
28. J. B. Keller, S. I. Rubinow, Slender-body theory for slow viscous flow, *J. Fluid Mech.* **75** (1976) 705–714.
29. E. Lauga, T. Powers, The hydrodynamics of swimming microorganisms, *Rep. Prog. Phys.* **72** (2009) 096601, http://dx.doi.org/10.1088/0034-4885/72/9/096601.
30. J. Lighthill, *Mathematical Biofluiddynamics*, SIAM, Philadelphia, 1975.
31. ———, Flagellar hydrodynamics, *SIAM Rev.* **18** (1976) 161–230.
32. I. Miyasaka, K. Nanba, K. Furuya, Y. Nimura, A. Azuma, Functional roles of the transverse and longitudinal flagella in the swimming motility of *Prorocentrum minimum* (Dinophyceae)., *J. Exp. Biol.* **207** (2004) 3055–3066.
33. M. J. Moritz, K. A. Schmitz, C. B. Lindemann, Measurement of the force and torque produced in the calcium response of reactivated rat sperm flagella, *Cell Motil. Cytoskeleton* **49** (2001) 33–40.
34. H. Nguyen, R. Ortiz, R. Cortez, L. Fauci, The action of waving cylindrical rings in a viscous fluid, *J. Fluid Mech.* **671** (2011) 574–586, http://dx.doi.org/10.1017/s0022112010006075.
35. S. D. Olson, S. S. Suarez, L. J. Fauci, Coupling biochemistry and hydrodynamics captures hyperactivated sperm motility in a simple flagellar model, *J. Theoretical Bio.* **283** (2011) 203–216.
36. C. Pozrikidis, *Boundary Integral and Singularity Methods for Linearized Viscous Flow*, Cambridge Univ. Press, 1992.
37. C. Pozrikidis, *Introduction to Theoretical and Computational Fluid Dynamics*, Oxford Univ. Press, 1997.
38. E. M. Purcell, Life at low Reynolds number, *Am. J. Phys.* **45** (1977) 3–11.
39. M. Roper, M. Dayel, R. Pepper, M. Koehl, Cooperatively generated stresslet flows supply fresh fluid to multicellular choanoflagellate colonies, *Phys. Rev. Lett.* **110** (2013) 228104, http://dx.doi.org/10.1103/physrevlett.110.228104.
40. D. J. Smith, A boundary element regularized Stokeslet method applied to cilia- and flagella-driven flow, *Proc. R. Soc. A* **465** (2009) 3605–3626.
41. D. J. Smith, E. A. Gaffney, J. R. Blake, J. C. Kirkman-Brown, Human sperm accumulation near surfaces: A simulation study, *J. Fluid Mech.* **621** (2009) 289–320.

42. H. A. Stone, A. D. Stroock, A. Ajdari, Engineering flows in small devices: Microfluidics toward a lab-on-a-chip, *Annu. Rev. Fluid Mech.* **36** (2004) 381–411.
43. G. I. Taylor, Analysis of the swimming of microscopic organisms, *Proc. R. Soc. Lond.* **209** (1951) 447.
44. A. K. Tornberg, M. Shelley, Simulating the dynamics and interactions of flexible fibers in Stokes flows, *J. Comput. Phys.* **196** (2004) 8–40.
45. S. Tottori, L. Zhang, K. K. Krawczyk, A. Franco-Obregon, B. J. Nelson, Magnetic helical micromachines: Fabrication, controlled swimming, and cargo transport, *Adv. Mater.* **24** (2012) 811–816, `http://dx.doi.org/10.1002/adma.201103818`.
46. D. B. Weibel, P. Garstecki, D. Ryan, W. R. DiLuzio, M. Meyer, J. E. Seto, G. M. Whitesides, Microoxen: Microorganisms to move microscale loads, *Proc. Natl. Acad. Sci.* **102** (2005) 11963–11967.
47. A. M. Young, L. Karp-Boss, P. A. Jumars, E. N. Landis, Quantifying diatom aspirations: Mechanical properties of chain-forming species, *Limnol. Oceanogr.* **57** (2012) 1789, `http://dx.doi.org/10.4319/lo.2012.57.6.1789`.
48. L. Zhang, J. Abbott, L. Dong, K. Peyer, B. Kratochvil, H. Zhang, C. Bergeles, B. J. Nelson, Characterizing the swimming properties of artificial bacterial flagella, *Nano Lett.* **9** (2009) 3663–3667.

HOA NGUYEN received her Ph.D. in computational and applied mathematics from Florida State University and then became a postdoctoral researcher at the Center for Computational Science at Tulane University. She is now an assistant professor of the Department of Mathematics at Trinity University in San Antonio, Texas. She is passionate about engaging undergraduate students in her research and enjoys collaborating with others to solve interesting problems in computational fluid dynamics, mathematical biology, multiscale modeling and simulations of protein aggregation and misfolding, mesh generation, and robotic navigation.
Department of Mathematics, Trinity University, San Antonio, TX 78212
hnguyen5@trinity.edu

RICARDO CORTEZ received a B.A. in mathematics and a B.S. in mechanical engineering from Arizona State University. He earned a Ph.D. in applied mathematics from the University of California at Berkeley in 1995 and became an NSF postdoctoral fellow and Courant Instructor at New York University. He joined the faculty at Tulane University in 1998, where he is the Pendergraft William Larkin Duren Professor of Mathematics and director of the Center for Computational Science. Prof. Cortez was the 2012 recipient of the Blackwell–Tapia prize for significant contributions to research and for serving as a role model for mathematical scientists and students from underrepresented minority groups. His research interests include computational mathematics, mathematical biology, modeling, and secondary mathematics education.
Mathematics Department, Tulane University, New Orleans, LA 70118
rcortez@tulane.edu

LISA FAUCI received her Ph.D. in Mathematics from the Courant Institute of New York University, and then joined the Department of Mathematics at Tulane University in New Orleans, Louisiana. She enjoys working with students and postdocs on problems in biological fluid dynamics and scientific computing.
Mathematics Department, Tulane University, New Orleans, LA 70118
fauci@tulane.edu